Optical Absorption and Computational Studies of [Ni]-Bacteriochlorophyll-*a*. New Insight into Charge Distribution between Metal and Ligands

Dror Noy,[†,‡] Roie Yerushalmi,[†,⊥] Vlad Brumfeld,[†] Idan Ashur,[†] Hugo Scheer,[||] Kim K. Baldridge,[#] and Avigdor Scherz*,[†]

Contribution from the Department of Plant Sciences, Weizmann Institute of Science, 76100 Rehovot, Israel, Botanisches Institut der Universität, D-80638 München, Germany, and Department of Chemstry, University of California, San Diego, California

Received October 20, 1999

Abstract: The relation between electronegativity and the electronic chemical potential provides new avenues for investigating chemical entities and their dynamics. One particular application concerns the tuning of biological redox centers consisting of metals and different ligands, where the effective charge at the metal center and the association and dissociation of the ligands play a key role. To quantify these factors we have recently synthesized a set of metal-substituted bacteriochlorophylls ([M]-BChls), whereby the caged metal can bind various axial ligands of biological significance and the BChl π-system is used as a "molecular potentiometer" to estimate the metal's effective charge. Here, we have concentrated on modifying this charge by axial ligation. We specifically selected [Ni]-BChl because (1) it forms three states of coordination with nitrogenous ligands, (2) Ni(II) has biological significance, and (3) [Ni]-porphyrins are extensively used for modeling [Fe]-porphyrins. The pure spectrum of each state of coordination and the equilibrium constants for monoligation ($K_1 = 5.6 \pm 0.2$ and 29.6 ± 1.1 M^{-1}) and biligation ($K_2 = 35.1 \pm 0.9$ and 26.8 ± 0.9 M^{-1}) of pyridine (Py) and imidazole (Im), respectively, were determined by factor analysis. Following the principle of electronegativity equalization and the model described in our previous paper (Noy, D.; Fiedor, L.; Hartwich, G.; Scheer, H.; Scherz, A. *J. Am. Chem. Soc.* **1998**, *120*, 3684−3693), we estimated that 0.30 and 0.27 electron charge units migrated from imidazole and pyridine, respectively, into the [Ni]-BChl central core upon monoligation. An additional, similar amount was transferred with the second ligation. High-level hybrid density functional theory (HDFT) calculations performed for [Ni]-BChl and [Ni]-BChl·Im in the gas phase were in very good agreement with the empirical results, suggesting that the [Ni]-BChl central core is enriched by 0.21 electron charge units upon ligation to a single Im molecule. Moreover, the Ni(II) covalent radius expanded by 0.07 and 0.09 Å upon monoligation and by 0.13 and 0.18 Å upon biligation with pyridine and imidazole, respectively. These results are in good agreement with X-ray data for ligated [Ni]-porphyrins (Jia, S. L.; Jentzen, W.; Shang, M.; Song, X. Z.; Ma, J. G.; Scheidt, W. R.; Shelnutt, J. A. *Inorg. Chem.* **1998**, *37*, 4402−4412) and our HDFT calculations (0.085 Å expansion upon Im monoligation). Line shape analyses of the Q_y bands indicated that the initial excited-state lifetimes of [Ni]-BChl were 75, 153, and 184 fs when ligated with zero, one, or two molecules of imidazole. The lifetimes for the analogous complexes with pyridine were 50% longer. Excitation of [Ni]-BChl·Py_2 caused dissociation of the ligands (in ∼100 ps), which recovered after a much longer time.

Introduction

Metal complexes are found in the active sites of many enzymes. They participate in catalysis of biochemical reactions as well as in the storage and transport of small molecules, ions, protons, and electrons.[1,2] Specific metal−ligand interactions, which frequently involve association and dissociation, are key factors that determine the functionality of the enzyme's active site, which can be either a metal (e.g., the heme iron in cytochromes[3]) or its ligands (e.g., the chlorophyll π-system in photosynthetic reaction centers[4]).

In many metalloenzymes a tetrapyrrole macrocycle occupies four of the metal's coordination sites. The remaining axial positions are occupied either by substrate molecules or by amino acid residues, the most common ones[2] being the thiolate of cysteins, the imidazole of histidines, the carboxylate of aspartic and glutamic acids, as well as the phenolate group of tyrosines. Metallotetrapyrroles, particularly metalloporphyrin derivatives, have been extensively studied not only for understanding their biological functions but also for investigating the fundamental aspects of metal−ligand interactions.[5−10] In this context, the

* To whom correspondence should be addressed.
† Weizmann Institute of Science.
‡ In partial fulfillment of this author's Ph.D. Thesis.
⊥ In partial fulfillment of this author's M.Sc. Thesis.
|| Botanisches Institute der Universität.
University of California.

(1) Bertini, I.; Gray, H. B.; Lippard, S. J.; Valentine, J. S. *Bioinorganic Chemistry*; University Science: Mill Valley, CA, 1994.
(2) Lippard, S. J.; Berg, J. M. *Principles of Bioinorganic Chemistry*; University Science: Mill Valley, CA, 1994.
(3) Chapman, S. K.; Daff, S.; Munro, A. W. *Struct. Bonding* **1997**, *88*, 39−70.
(4) Evans, M. C. W.; Nugent, J. H. A. In *The Photosynthetic Reaction Center*; Deisenhofer, J., Norris, J. R., Eds.; Academic Press: 1993; Vol. I, pp 391−415.
(5) Cole, S. J.; Curthoys, G. C.; Magnusson, E. A.; Philips, J. N. *Inorg. Chem.* **1972**, *11*, 1024−1028.

10.1021/ja993761e CCC: $19.00
Published on Web 04/06/2000

optical spectra and redox behavior of metalloporphyrins have often been used to follow the interactions between a metal caged by the pyrrolic macrocycle and various biologically relevant axial ligands. However, because the porphyrins' major electronic transitions are degenerate, the interpretation of experimental data is complicated.[11−13] As a result, the effect of axial ligation on the redox behavior of metalloporphyrins has not yet been sufficiently understood.

Electronegativity, defined as the chemical potential of an electron within an atom or a chemical group, provides a means to estimate such effects even in large and complex systems such as redox proteins.[14,15] When two chemical entities interact, their electron densities redistribute until their electronegativities equalize.[16−18] Therefore, redox potential tuning can be described in terms of electronegativity equalization between different chemical groups such as coordinated metals and their ligands.

Many years ago Gouterman[19] and later Fuhrhop et al.[20] described the linear correlation between spectroscopic transitions and redox potentials of metal-substituted porphyrins and the electronegativities of their incorporated metals. However, changes in the electronegativity of a particular metal upon ligand binding (as a result of electronegativity equalization) were not considered. Such changes should also be reflected in the electronic transitions and redox potentials of the porphyrin's π-system. Unfortunately, the resolution of $\pi-\pi$ transitions in D_{4h} porphyrins is insufficient for quantifying these relationships.

Recently, we have introduced metal-substituted BChls ([M]-BChls), a group of reduced metalloporphyrins with highly resolved $\pi-\pi^*$ transition energies and redox potentials.[21] We followed Gordy's definition of electronegativity in its modern formulation[22] and showed that changes in the electronic spectra and redox potentials upon metal substitution can be accounted for in terms of electrostatic interactions between the effective charge at the metal center and the π-electron density of the macrocycle.[23] Consequently, the π-electron system of BChl can be used as a molecular "potentiometer" whereby the electrostatic potential at the metal center is monitored by the electronic spectra and redox potentials of the [M]-BChl's π-system.

Here, we have used [Ni]-BChl for monitoring charge migration into and out of a metal center as a result of axial ligation. By monitoring changes in the metal's effective charge, we obtained information about the electronic properties of the ligand. [Ni]-BChl was chosen because data from in vitro and in vivo experiments showed that it could be found at three states of coordination. It was monoligated in reconstituted bacterial reaction centers (RCs),[24] whereas the biligated and nonligated forms were observed in coordinating and noncoordinating solvents, respectively.[21,23] The Q_x transition energies of each species were substantially different and provided information about the particular state of coordination. We have shown that when small amounts of nitrogenous ligands such as pyridine (Py) and imidazole (Im) are added to a solution of [Ni]-BChl in acetonitrile (AN), all three coordination states are in thermodynamic equilibrium. The characteristic electronic spectrum of each state of coordination and the respective axial ligation constants were derived from spectrophotometric titrations through modeling factor analysis.[25] We used the resolved spectra to quantitatively estimate charge migration from the axial ligands to the central metal based on electronegativity equalization considerations. As a first test case we compared the semiempirical results with high-level hybrid density functional theory (HDFT) calculations for nonligated and monoligated [Ni]-BChl. We have also examined some kinetic aspects of axial ligand photodissociation as a consequence of excitation of the BChl macrocycle.

Materials and Methods

[Ni]-BChl was prepared according to Hartwich et al.[21] AN and Py (Aldrich) were dried over activated 3A molecular sieves (Sigma) according to Burfield et al.,[26,27] degassed, and transferred under vacuum. Solutions of Im (Sigma) in dry AN were prepared just before measuring. All the sample preparations were carried out in a glovebox under inert and dry atmosphere.

Absorption spectra of [Ni]-BChl in dry AN were recorded in a standard 10-mm quartz cuvette using a Cary 5 UV-Vis-IR double-beam spectrophotometer. The cuvette was sealed with a Teflon-coated septum stopper through which Py or Im was injected with a microliter syringe.

Time-resolved absorption spectroscopy of [Ni]-BChl dissolved in 0.5 mL of diethyl ether (DE) that contained millimolar concentrations of Py (DE/Py) was carried out using a pump−probe setup. Samples were measured in a 2-mm quartz cuvette sealed with a Teflon stopper to prevent evaporation of solvents. The sample was excited at 690 nm by 14-ps 90-mJ pulses generated from a Continuum PD10 dye laser that was pumped by a frequency-doubled Nd:YAG laser (532 nm, 38 ps). White-light pulses (480−860 nm), generated by focusing the residual fundamental beam (1064 nm, 38 ps) of the Nd:YAG laser on a 5-cm path length cylindrical water cell, were used for probing. The pump−probe interval was controlled by an optical delay line. Spectra were detected using a double diode array (DIDA 512) with dedicated software (Winspec), all from Princeton Instruments. Pump pulse intensity was monitored by a power meter (Coherent LabMaster). The measurement accuracy was about 0.01 absorbance units.

Resolving the Optical Absorption Spectrum of [Ni]-BChl at Each State of Coordination. Analysis of the digitized spectra was carried out with Matlab software using custom programs as well as Matlab's standard optimization and statistics toolboxes.

Modeling factor analysis was used for separating the overlapping spectra of [Ni]-BChl in the different states of coordination. The

(6) Walker, F. A.; Beroiz, D.; Kadish, K. M. *J. Am. Chem. Soc.* **1976**, *98*, 3484−3489.
(7) Rodriguez, J.; Holten, D. *J. Phys. Chem.* **1990**, *92*, 5944−5950.
(8) Scheidt, W. R.; Lee, Y. J. *Struct. Bonding* **1987**, *64*, 1−70.
(9) Kadish, K. M.; Bottomley, L. A. *Inorg. Chem.* **1980**, *19*, 832−836.
(10) Kadish, K. M.; Bottomley, L. A.; Kelly, S.; Schaeper, D.; Shiue, L. R. *J. Electroanal. Chem.* **1981**, *128*, 213−222.
(11) Hanson, L. K. In *Chlorophylls*; Scheer, H., Ed.; CRC Press: Boca Raton, FL, 1991; pp 993−1014.
(12) Gouterman, M.; Wagniere, G. H.; Snyder, L. C. *J. Mol. Spectrosc.* **1963**, *11*, 108−127.
(13) Gouterman, M. *J. Mol. Spectrosc.* **1961**, *6*, 138−163.
(14) York, D. M.; Yang, W. T. *J. Chem. Phys.* **1996**, *104*, 159−172.
(15) Liu, Y. P.; Kim, K.; Berne, B. J.; Friesner, R. A.; Rick, S. W. *J. Chem. Phys.* **1998**, *108*, 4739−4755.
(16) Sanderson, R. T. *J. Chem. Educ.* **1952**, *29*, 539−544.
(17) Sanderson, R. T. *J. Chem. Educ.* **1954**, *31*, 2−7.
(18) Parr, R. G.; Donnely, R. A.; Levy, M.; Palke, W. E. *J. Chem. Phys.* **1978**, *68*, 3801−3807.
(19) Gouterman, M. *J. Chem. Phys.* **1959**, *30*, 1139−1161.
(20) Fuhrhop, J. H.; Kadish, K. M.; Davis, D. G. *J. Am. Chem. Soc.* **1973**, *95*, 5140−5147.
(21) Hartwich, G.; Fiedor, L.; Simonin, I.; Cmiel, E.; Schafer, W.; Noy, D.; Scherz, A.; Scheer, H. *J. Am. Chem. Soc.* **1998**, *120*, 3675−3683.
(22) Gordy defined the electronegativity of an atom as the electrostatic potential at its covalent radius due to effective nuclear charge (Gordy, W. *Phys. Rev.* **1946**, *69*, 604−607). This definition was verified 37 years later by Politzer et al. (Politzer, P.; Parr, R. G.; Murphy, D. R. *J. Chem. Phys.* **1983**, *79*, 3859−3861) using density functional theory.
(23) Noy, D.; Fiedor, L.; Hartwich, G.; Scheer, H.; Scherz, A. *J. Am. Chem. Soc.* **1998**, *120*, 3684−3693.
(24) Chen, L. X.; Wang, Z. Y.; Hartwich, G.; Katheder, I.; Scheer, H.; Scherz, A.; Montano, P. A.; Norris, J. R. *Chem. Phys. Lett.* **1995**, *234*, 437−444.
(25) Malinowski, E. R. *Factor Analysis in Chemistry*, 2nd ed.; Wiley: New York, 1991.
(26) Burfield, D. R.; Lee, K. H.; Smithers, R. H. *J. Org. Chem.* **1977**, *42*, 3060−3065.
(27) Burfield, D. R.; Smithers, R. H.; Tan, A. S. C. *J. Org. Chem.* **1981**, *46*, 629−631.

evolution model considers two equilibrium constants

$$\text{[Ni]-BChl} + \text{L} \rightleftarrows \text{[Ni]-BChl·L} \qquad K_1$$

$$\text{[Ni]-BChl·L} + \text{L} \rightleftarrows \text{[Ni]-BChl·L}_2 \qquad K_2 \tag{1}$$

The mole fraction, p_{ij}, of each coordination state is expressed as a function of the axial ligation constants K_1 and K_2 and the ligand concentration $[L]_j$, in the jth sample

$$p_{1j} = 1/\Delta$$

$$p_{2j} = K_1 \cdot [L]_j/\Delta$$

$$p_{3j} = K_1 \cdot K_2 \cdot [L]_j^2/\Delta \tag{2}$$

where $\Delta = 1 + K_1 \cdot [L]_j + K_1 \cdot K_2 \cdot [L]_j^2$ and the indices 1, 2, and 3 correspond to [Ni]-BChl, [Ni]-BChl·L, and [Ni]-BChl·L_2, respectively. The constants K_1 and K_2 were optimized by searching for $\{p_{ij}\}$, which minimizes the root-mean-square error (RMSE) in the data reproduction given by[25]

$$\text{RMSE} = \sqrt{\sum_{k=1}^{n}\sum_{j=1}^{m}(d_{kj} - \sum_{i=1}^{3} s_{ki} \cdot p_{ij})^2/(m \cdot n)} \tag{3}$$

where $\{d_{kj}\}$ represents the absorbance of the jth sample at the kth wavelength and constitutes the elements of the experimental data matrix, **D**. The pure spectral components matrix, **S**, in which an element, s_{ki}, represents the absorbance of the ith coordination state at the kth wavelength was calculated by using the pseudoinverse of the $\{p_{ij}\}$ matrix, $\mathbf{P}^+$,

$$\mathbf{S} = \mathbf{D} \cdot \mathbf{P}^+ \tag{4}$$

Confidence intervals for K_1 and K_2 were calculated according to O'Dea et al.[28] Substituting these intervals into eqs 2 and 4 yielded confidence intervals for the mole fractions and pure spectral components, respectively.

Estimating the Q_y Singlet Excited-State Lifetime. The Q_y transition bands of pure [Ni]-BChl, [Ni]-BChl·Py, [Ni]-BChl·Py_2, [Ni]-BChl·Im, and [Ni]-BChl·Im_2 were symmetrized by mirroring their low energy half about the center of the band. This treatment assured that only the 0−0 electronic transition contributed to the line shape and circumvented complications arising from mixing high-frequency vibronic states. Following Cupane et al.,[29−31] the symmetrized band was described by a Voigt function

$$V(\nu) = M^2 \cdot \nu \cdot S \cdot G(\nu) \otimes L(\nu_0(T) - \nu) \tag{5a}$$

where $\otimes$ is the convolution operator, ν denotes frequency, $\nu_0(T)$ is the temperature-dependent transition frequency, and the constants M and S are proportional to the electronic dipole matrix element and the vibronic coupling factor, respectively. The Gaussian component

$$G(\nu) = 1/\sigma(T) \cdot \exp[-\nu^2/2\sigma^2(T)] \tag{5b}$$

describes the effect of inhomogeneous broadening, where the temperature-dependent parameter, $\sigma(T)$, determines the Gaussian full width at half-maximum [$\text{FWHM}_G = 2\sigma(T) \cdot \sqrt{\ln(4)}$]. The full width at half-maximum of the Lorentzian component,

$$L(\nu_0(T) - \nu) = (1/2\tau)/[(\nu_0(T) - \nu)^2 + (1/2\tau)^2] \tag{5c}$$

is determined by the excited-state finite lifetime, τ ($\text{FWHM}_L = 1/\tau$).

The parameters τ and $\sigma(T)$ were estimated by fitting eq 5 to the symmetrized Q_y bands by using PeakFit software.

Estimating the Changes in Electronegativity, Covalent Radius, and Effective Charge at the Central Metal. The changes in electronegativity, $\Delta\chi$, covalent radius, Δr, and effective charge, ΔQ^o, were estimated by applying the model derived in our previous work for [M]-BChls.[23] The model is given in matrix notation by

$$\Delta\mathbf{E} = \mathbf{R} \cdot \mathbf{L} \tag{6}$$

where the rows of the experimental data matrix, $\Delta\mathbf{E}$, correspond to the [M]-BChl species and the columns to changes in the main four transition energies (B_y, B_x, Q_x, and Q_y) and redox potentials. The respective values of $\Delta\chi$ and Δr are arranged in the columns of the scores matrix, **R**. The loading matrix, **L**, contains the respective loading coefficients of $\Delta\chi$ and Δr.

Here, the changes in electronegativity and covalent radius upon adding axial ligands to the central Ni(II) atom are given by

$$\mathbf{R} = \Delta\mathbf{E} \cdot \mathbf{L}^+ \tag{7}$$

where $\Delta\mathbf{E}$ represents the changes in the electronic transition energies of the axially ligated [Ni]-BChl species with respect to nonligated [Ni]-BChl, and $\mathbf{L}^+$ is the pseudoinverse of **L**, which contains the loading coefficients, $l_{\chi,N}$ and $l_{r,N}$, from ref 23. Changes in the effective positive charge were calculated by eq 29 in ref 23

$$\Delta Q^o = 0.12 \cdot \Delta\chi \tag{8}$$

Quantum Mechanical Methods. Molecular structures were obtained by employing HDFT techniques,[32] using the algorithms contained with the GAUSSIAN98 package.[33] The HDFT functional used was the B3LYP[34] functional which employs the Lee−Yang−Parr correlation functional[35] in conjunction with a hybrid exchange functional first proposed by Becke.[36] HDFT techniques are particularly important for studying structures of the size considered here, since they implicitly include electron correlation effects at a great saving in computer time compared with the conventional methods. The size of the complexes involved and the presence of the transition metal influenced our choice of basis set. The Hay and Wadt relativistic effective core potentials (RECP)[37] were employed for the Ni atom. Specifically, the effective core potential/basis set combination used was LANL2DZ (Los Alamos National Laboratory 2-double-ζ; the "2" indicating that the valence and "valence-1" shells are treated explicitly).[38] The LANL2DZ basis set is of double-ζ quality in the valence and "valence-1" shells, whereas the RECP contains Darwin and mass-velocity contributions.[37,39,40] Using

(28) O'Dea, J.; Osteryoung, J.; Lane, T. *J. Phys. Chem.* **1986**, *90*, 2761−2764.
(29) Cupane, A.; Leone, M.; Vitrano, E.; Cordone, L. *Eur. Biophys. J.* **1995**, *23*, 385−398.
(30) Cupane, A.; Leone, M.; Cordone, L.; Gilch, H.; Dreybrodt, W.; Unger, E.; Schweitzer-Stenner, R. *J. Phys. Chem.* **1996**, *100*, 14192−14197.
(31) Cupane, A.; Leone, M.; Unger, E.; Lemke, C.; Beck, M.; Dreybrodt, W.; Schweitzer-Stenner, R. *J. Phys. Chem. B* **1998**, *102*, 6612−6620.
(32) Parr, R. G.; Yang, W. *Density Functional Theory of Atoms and Molecules*; Oxford University Press: New York, 1989.
(33) Frisch, M. J.; Trucks, G. W.; Schlegel, H. B.; Scuseria, G. E.; Robb, M. A.; Cheeseman, J. R.; Zakrzewski, V. G.; Montgomery, J. A. J.; Stratmann, R. E.; Burant, J. C.; Dapprich, S.; Millam, J. M.; Daniels, A. D.; Kudin, K. N.; Strain, M. C.; Farkas, O.; Tomasi, J.; Barone, V.; Cossi, M.; Cammi, R.; Mennucci, B.; Pomelli, C.; Adamo, C.; Clifford, S.; Ochterski, J.; Petersson, G. A.; Ayala, P. Y.; Cui, Q.; Morokuma, K.; Malick, D. K.; Rabuck, A. D.; Raghavachari, K.; Foresman, J. B.; Cioslowski, J.; Ortiz, J. V.; Stefanov, B. B.; Liu, G.; Liashenko, A.; Piskorz, P.; Komaromi, I.; Gomperts, R.; Martin, R. L.; Fox, D. J.; Keith, T.; Al-Laham, M. A.; Peng, C. Y.; Nanayakkara, A.; Gonzalez, C.; Challacombe, M.; Gill, P. M. W.; Johnson, B.; Chen, W.; Wong, M. W.; Andres, J. L.; Gonzalez, C.; Head-Gordon, M.; Replogle, E. S.; Pople, J. A. *GAUSSIAN 98*, Revision A.6; Gaussian, Inc.: Pittsburgh, PA, 1998.
(34) Barone, V. *Chem. Phys. Lett.* **1994**, *226*, 392−398.
(35) Lee, C.; Yang, W.; Parr, R. G. *Phys. Rev.* **1988**, *B37*, 785−789.
(36) Becke, A. D. *J. Chem. Phys.* **1993**, *98*, 5648−5652.
(37) Hay, P. J.; Wadt, W. R. *J. Chem. Phys.* **1985**, *82*, 299−310.
(38) Dunning, T. H., Jr.; Hay, P. J. *Modern Theoretical Chemistry*; Plenum: New York, 1976.
(39) Hay, P. J.; Wadt, W. R. *J. Chem. Phys.* **1985**, *82*, 270−283.
(40) Wadt, W. R.; Hay, P. J. *J. Chem. Phys.* **1985**, *82*, 284−298.

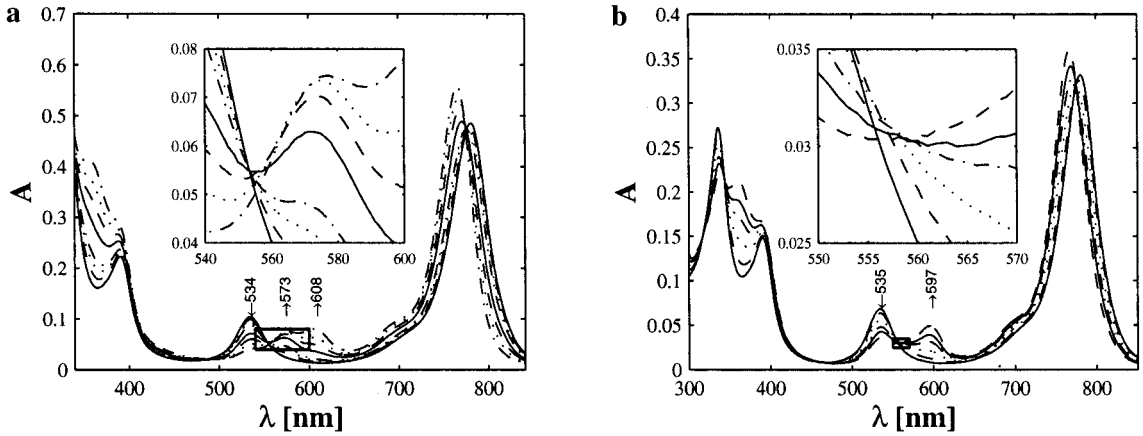

Figure 1. Spectroscopic titration of [Ni]-BChl in AN with Im (a) and Py (b).

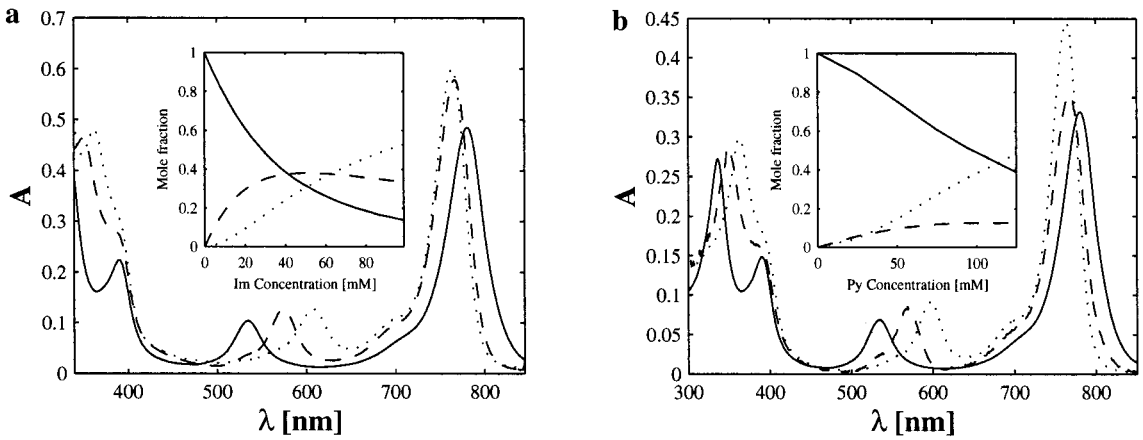

Figure 2. Spectral components and relative concentrations (inset) of nonligated (—), monoligated (− −), and biligated (•••) [Ni]-BChls obtained by applying modeling factor analysis on the spectroscopic titrations of [Ni]-BChl in AN with Im (a) and Py (b).

RECP has been found to be computationally very efficient and reliable for handling relativistic effects, which must be accounted for in the complexes involving Ni atoms.[41]

While this choice of basis set combination is sufficient for the types of comparisons made here, our preliminary studies (data not shown) reveal a general tendency of this particular double-ζ basis set to overestimate C−N bond lengths by approximately 1.7−2.0 pm due to the lack of polarization functionality. One can easily remedy this effect for first and second row elements by increasing the basis set. However, since here we focus on bond length *differences* rather than absolute values, we have chosen to keep this basis set combination for the present structural analysis with the knowledge that C−N bonds will be slightly longer, investing further computational efforts in computing electronic properties. We are pursuing more rigorous structural investigations on a larger series of [M]-BChl complexes to determine an optimal basis set combination, which will provide more absolute consistency across all bond types while maintaining computational efficiency.

For more accurate determination of electronic properties, single point energy calculations were carried out using a larger basis set denoted LANL2DZ+1, which consists of the LANL2DZ basis set augmented with a single set of f functions (exponents determined by Frenkling and co-workers[42,43]) on Ni, and the standard Dunning's cc-pvdz (correlation consistent polarized valence double-ζ) basis set[44] ([4s3p1d/3s2p1d/2s1p]) on first and second row atoms.

Atomic charges were derived from a least-squares fit to the electrostatic potential (ESP), calculated at points selected according to the Merz−Singh−Kollman scheme,[45,46] and subject to the constraint of constant total molecular charge. Many points are thus chosen on nested Connolly surfaces with a density of 1 point/Å. The method samples points at 1.4, 1.6, 1.8, and 2.0 times the van der Waals radius of the atoms. An atomic radius of 1.63 Å was used for Ni.

Results

The Optical Absorption Spectrum of [Ni]-BChl at Each State of Coordination. Figure 1 presents the evolution of [Ni]-BChl absorption spectra in AN to which Im (part a) and Py (part b) were added. With the addition of Im, a distinct absorption band increased at 573 nm, characteristic of the Q_x transition of monoligated [M]-BChl (Figure 1a, inset). When more Im was added, the biligated form appeared with the characteristic Q_x absorption band at 608 nm. With Py, the Q_x band shifted from 535 to 597 nm with increasing ligand concentration, which is characteristic of biligation. No clear band could be observed at 560−580 nm, but there was a systematic red shift of the "isosbestic" point in that region (Figure 1b, inset).

Table 1 and Figure 2 present the spectra of non-, mono-, and biligated [Ni]-BChl with Im (part a) and Py (part b) ligands as well as their binding constants derived by modeling factor analysis (eqs 2−4). The quality of data reproduction was at the

(41) Siegbahn, P. E. M. *Adv. Chem. Phys.* **1996**, *93*, 333−387.
(42) Ehlers, A. W.; Bohme, M.; Dapprich, S.; Gobbi, A.; Hollwarth, A.; Jonas, V.; Kohler, K. F.; Stegmann, R.; Veldkamp, A.; Frenking, G. *Chem. Phys. Lett.* **1993**, *208*, 111−114.
(43) Hollwarth, A.; Bohme, M.; Dapprich, S.; Ehlers, A. W.; Gobbi, A.; Jonas, V.; Kohler, K. F.; Stegmann, R.; Veldkamp, A.; Frenking, G. *Chem. Phys. Lett.* **1993**, *208*, 237−240.
(44) Dunning, T. H. *J. Chem. Phys.* **1989**, *90*, 1007−1023.
(45) Besler, B. H.; Merz, K. M.; Kollman, P. A. *J. Comput. Chem.* **1990**, *11*, 431−439.
(46) Singh, U. C.; Kollman, P. A. *J. Comput. Chem.* **1984**, *5*, 129−145.

Table 1. Binding Constants for the First (eq 1, K_1) and Second (eq 1, K_2) Ligands, Absorption Characteristics, Temperature-Dependent Inhomogeneous Broadening [σ(T)], and Initial Excited State Lifetimes (τ) of Non-, Mono-, and Biligated [Ni]-BChl

	[Ni]-BChl	[Ni]-BChl·Py	[Ni]-BChl·Im	[Ni]-BChl·Py_2	[Ni]-BChl·Im_2
K_L [M^{-1}]		5.6 ± 0.2	29.6 ± 1.1	$35.1 + 0.8/-0.9$	26.8 ± 0.9
B_y [nm]	337	350	350	363	362
B_x [nm]	391	391	391	391	391
Q_x [nm]	535	569	573	597	608
Q_y [nm]	780	767	767	764	764
$\sigma(T)$ [cm^{-1}][a]	199 ± 4	242 ± 3	230 ± 2	214 ± 2	203 ± 2
τ [fs][a]	75 ± 2	235 ± 10	153 ± 6	308 ± 13	184 ± 6

[a] Obtained by fitting eq 5 to the symmetrized Q_y band.

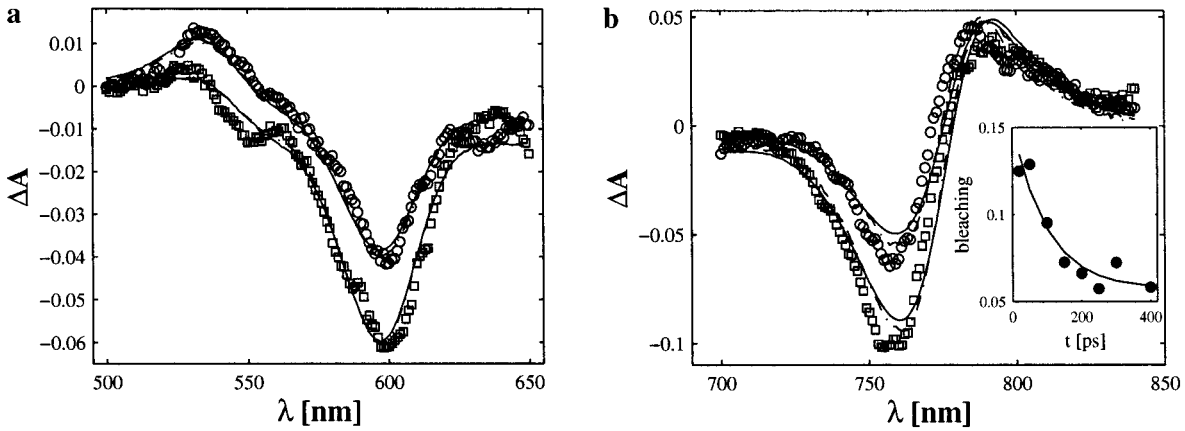

Figure 3. Difference absorption spectra of the Q_x (a) and Q_y (b) regions of [Ni]-BChl in DE/Py 50 ps (□) and 200 ps (○) after excitation. The spectra were simulated by linear combination either of non- and biligated [Ni]-BChl (—) or non-, mono-, and biligated [Ni]-BChls (— —). The kinetics of Q_y bleaching (inset) is single exponential with a lifetime of 100 ps.

spectrophotometric accuracy level of the Cary 5 (RMSE = 3×10^{-4} and 4×10^{-4} absorbance units for the Py and Im titrations, respectively).

The resolved [Ni]-BChl spectra were characteristic of [M]-BChls.[21,23] The energy of the Q_x transition showed the highest sensitivity to the coordination state: it shifted to the red from 534 nm for [Ni]-BChl to 569 nm in [Ni]-BChl·Py and increased to 597 nm for [Ni]-BChl·Py_2. The ligand effect was even larger when Im was added (573 and 608 for [Ni]-BChl·Im and [Ni]-BChl·Im_2, respectively). The Q_y transition band blue shifted from 780, 767, and 764 nm in the non-, mono-, and biligated species, respectively.

Nitrogenous Ligand Binding to [Ni]-BChl in AN. Table 1 presents the axial ligation constants of Py and Im. The low RMSE values and narrow confidence intervals indicate that the model described in eqs 1 and 2 accurately represents the evolution of [Ni]-BChl coordination states during the titrations. Note that the axial ligation of either AN or residual water seems to be negligible. Additionally, the binding constant of the first Py (K_1) is substantially smaller than the binding constant of the second Py (K_2), which accounts for the low concentrations of [Ni]-BChl·Py throughout the titration. With Im, K_1 is slightly larger than K_2. As a result, monoligated [Ni]-BChl significantly contributes to the absorption spectra even at high Im concentrations, and can be observed directly.

Lifetimes of the Q_y-Excited Singlet State in Different States of Coordination. Table 1 presents the results of fitting the symmetrized Q_y transition bands of pure [Ni]-BChl, [Ni]-BChl·Py, [Ni]-BChl·Py_2, [Ni]-BChl·Im, and [Ni]-BChl·Im_2 with the Voigt function in eq 5. The widths of the Gaussian components are almost constant (with a relative standard deviation of 8%) as expected from temperature-dependent inhomogeneous broadening.[30] However, the widths of the Lorentzian components vary considerably, indicating that excited-state lifetimes depend both on the state of ligation and the type of axial ligand. The shortest lifetime, 75 fs, was observed for nonligated [Ni]-BChl and the longest, 308 fs, for [Ni]-BChl·Py_2. Intermediate lifetimes of 153, 184, and 235 fs were observed for [Ni]-BChl·Im, [Ni]-BChl·Im_2, and [Ni]-BChl·Py, respectively.

Time-Resolved Absorption Spectroscopy of [Ni]-BChl in the Presence of Pyridine. Figure 3 shows typical difference absorption spectra of [Ni]-BChl in DE/Py, 50 and 200 ps after excitation at 690 nm with a 14-ps pump pulse. The ground-state recovery of [Ni]-BChl in pure DE was too fast to be detected by the 38-ps probe.[47,48] The Q_y (763 nm) and Q_x (597 nm) absorption bands of [Ni]-BChl·Py_2 bleached and did not completely recover even after 400 ps. During that time, two new absorption bands developed at 534 and 780 nm, corresponding to the Q_x and Q_y bands of nonligated [Ni]-BChl, respectively. We were able to reasonably simulate the difference spectra by using linear combinations of the pure [Ni]-BChl and [Ni]-BChl·Py_2 spectra (Figure 3, solid lines). Adding the spectrum of [Ni]-BChl·Py to the simulation did not improve its quality (Figure 3, dashed lines). The kinetics of ground-state recovery from 0 to 400 ps could be described by a single-exponential decay with a time constant of about 100 ps (Figure 3b, inset).

HDFT Calculations of [Ni]-BChl and [Ni]-BChl·Im. The calculated change in charge density and size of the [Ni]-BChl central core (central Ni atom and four BChl nitrogens) upon ligation with a single Im molecule are shown in Table 2. Structures were fully optimized with HDFT methods as detailed

(47) Rodriguez, J.; Holten, D. *J. Phys. Chem.* **1989**, *91*, 3525−3531.
(48) Musewald, C.; Hartwich, G.; Lossau, H.; Gilch, P.; Pollinger-Dammer, F.; Scheer, H.; Michel-Beyerle, M. E. *J. Phys. Chem. B* **1999**, *103*, 7055−7060.

Table 2. Changes in Transition Energies, Central Metal Electronegativity, Covalent Radius, and Effective Positive Charge of Mono- and Biligated [Ni]-BChl with Respect to the Nonligated Species

	[Ni]-BChl·Py	[Ni]-BChl·Im	[Ni]-BChl·Py_2	[Ni]-BChl·Im_2
ΔB_y [eV]	−0.14	−0.14	−0.27	−0.26
ΔB_x [eV]	0.00	0.00	0.00	0.00
ΔQ_x [eV]	−0.14	−0.16	−0.24	−0.28
ΔQ_y [eV]	0.03	0.03	0.03	0.03
$\Delta\chi$ [eV][a]	−2.24	−2.46	−3.89	−4.46
Δr [Å][a]	0.09	0.07	0.18	0.13
ΔQ^o [e^-][b]	−0.27	−0.30	−0.47	−0.54
ΔQ^o_{core} [e^-][c]		−0.21		
ΔQ^o_{ligand} [e^-][d]		0.23		
Δr_{core} [Å][e]		0.085		

[a] From eq 7. [b] From eq 8. [c] Difference between the MK-ESP calculated charge of monoligated and nonligated [Ni]-BChl cores (central Ni and four nitrogen atoms). [d] Difference between the MK-ESP calculated charge of free Im and Im ligated to [Ni]-BChl. [e] Difference between the mean Ni−N distance in monoligated and nonligated [Ni]-BChls.[49]

in the Materials and Methods section. Both singlet and triplet states were considered for the [Ni]-BChl·Im. The resulting energy difference between the two states is 12.4 kcal/mol at this level of theory, indicating that the [Ni]-BChl·Im ground state is a triplet state. Details of the structure show that the singlet state has a twisted conformation with the Ni remaining in the plane of the macrocycle, whereas the triplet state retains planarity, with the Ni slightly out of plane. The distance from the Ni to the axial imidazole ligand is nearly 2.06 Å in the triplet state, whereas the Ni−Im distance in the singlet state is 0.7 Å greater.[49]

Comparing [Ni]-BChl to [Ni]-BChl·Im reveals a binding energy of 16.6 kcal/mol, typical of experimental values. Upon ligation of Im, the metal center expands considerably. The mean distance from the Ni to the macrocycle nitrogens obtained from the optimized structures of [Ni]-BChl and [Ni]-BChl·Im is 2.0056 and 2.0901 Å, respectively, indicating an increase of 0.085 Å upon ligation as reported in Table 2.[49]

The Merz−Kollman electrostatic potential (MK-ESP) method of determining atomic charges has been employed for all computed structures. This method has been shown to give both excellent electrostatic moments as well as electrostatic potentials.[50] In addition, the prediction of such charges using the B3LYP HDFT method has been shown to be in excellent agreement with high-level conventional, dynamically correlated schemes (e.g., MP2, etc.).[51] MK-ESP computations were carried out on both the nonligated and monoligated optimized structures. The results indicate that the monoligated core is 0.21 e^- richer than the nonligated core, in agreement with our empirical model. Accordingly, the Im ligand is 0.23 e^- poorer when compared with isolated Im.

Discussion

Axial Ligation to [Ni]-BChl. [Ni]-porphyrins and [Ni]-BChl with only one axial ligand have been observed only in reconstituted hemoglobin[52] and bacterial RCs,[24] respectively. To the best of our knowledge, the electronic absorption spectrum of a pure monoligated [Ni]-porphyrin was never resolved in vitro.[53] This is partly because the degeneracy of optical transitions in D_{4h} porphyrins makes the interpretation of the experimental results difficult.[11−13,19]

The binding constant of the first Py is about six times smaller than the binding constant of the first Im, whereas the binding constant of the second Py is larger than the binding constant of the second Im. This phenomenon may reflect a larger trans influence[54] of Im with respect to Py. The subject is currently being investigated with a larger series of ligands.

The advantage of using reduced porphyrins such as BChls for studying metal coordination is that each state of ligation is characterized by a well-resolved Q_x band:[21,23] non-, mono-, and biligated [M]-BChls absorb at 530−550, 560−580, and 590−620 nm, respectively. Another advantage is the enhanced flexibility of the macrocycle with respect to D_{4h} porphyrins. This flexibility enables core expansion upon axial ligation, which is especially important for the binding of Im, a common nucleophilic biological ligand. In fact Im ligation to D_{4h} [Ni]-porphyrins is unusual in vitro,[55] whereas reduced porphyrins such as [Ni]-tri-β-oxoporphyrin bind it readily.[56] In our previous paper,[23] we claimed that core expansion is sufficient to account for the effect of macrocycle distortion on [M]-BChl's optical spectra. The good agreement between the core expansion derived here from optical spectra and that calculated by HDFT supports this assumption. Both HDFT-calculated core expansion and the empirically derived increase in the Ni(II) covalent radius (Table 2) are in good agreement with recent results from the literature based on crystal structure, Raman spectra, and force-field calculations,[57] which indicate an increase of about 0.1 Å in the core size of [Ni]-TPP upon binding the first axial ligand. This increase has been assigned to a change of the metal's d electron configuration. In the nonligated [Ni]-BChl complex (square planar), the Ni(II) is in a low-spin electronic configuration, where the d_{z^2} orbital is doubly occupied and the $d_{x^2-y^2}$ orbital is empty.[58] In terms of ligand-field theory,[2] the interaction between the lone pair electrons of the axial ligand and the electrons that occupy the d_{z^2} orbital raises the energy of the latter close to the empty $d_{x^2-y^2}$ energy level. When the energy gap between d_{z^2}

(49) As pointed out in the Quantum mechanical methods section, using the double-ζ basis sets results in slightly overestimated bond lengths. Nevertheless, relative values are accurately assessed because this effect is constant and all the structures are treated similarly. We are actively pursuing more accurate basis set combinations for handling [M]-BChl derivatives

(50) Sigfridsson, E.; Ryde, U. *J. Comput. Chem.* **1998**, *19*, 377−395.

(51) DeProft, F.; Martin, J. M. L.; Geerlings, P. *Chem. Phys. Lett.* **1996**, *250*, 393−401.

(52) Shelnutt, J. A.; Alston, K.; Ho, J. Y.; Yu, N. T.; Yamamoto, T.; Rifkind, J. M. *Biochemistry* **1986**, *25*, 620−627.

(53) The most direct evidence for the formation of monoligated porphyrin in solution was recently observed in the Raman spectra of [Ni]-TPP (Jia, S. L.; Jentzen, W.; Shang, M.; Song, X. Z.; Ma, J. G.; Scheidt, W. R.; Shelnutt, J. A. *Inorg. Chem.* **1998**, *37*, 4402−4412).

(54) Cotton, F. A.; Wilkinson, G. *Advanced Inorganic Chemistry*, 5th ed.; Wiley: New York, 1988.

(55) Pasternack, R. F.; Spiro, E. G.; Teach, M. *J. Inorg. Nucl. Chem.* **1974**, *36*, 599−606.

(56) Connick, P. A.; Haller, K. J.; Macor, K. A. *Inorg. Chem.* **1993**, *32*, 3256−3264.

(57) Jia, S. L.; Jentzen, W.; Shang, M.; Song, X. Z.; Ma, J. G.; Scheidt, W. R.; Shelnutt, J. A. *Inorg. Chem.* **1998**, *37*, 4402−4412.

(58) Ake, R. L.; Gouterman, M. *Theor. Chim. Acta* **1970**, *17*, 408−416.

and $d_{x^2-y^2}$ becomes smaller than the electron repulsion energy, the high-spin configuration in which one electron is promoted from d_{z^2} to $d_{x^2-y^2}$ becomes favorable. Electronegativity equalization theory provides an alternative approach whereby the redistribution of the metal's electrons is induced by the contribution of electron density from the ligand to the metal and is not necessarily confined to d-orbitals.

The Amount of Charge Exchanged by a Ligand and Metal Center. We have recently utilized the correlation between electronegativity and electrostatic potential for calculating the amount of net charge at the center of [M]-BChls.[23] The charge can be changed either by modifying the incorporated metal or, because of electronegativity equalization, by binding different ligands to the same metal. Here, we monitored charge modifications at the center of [Ni]-BChl in the presence of two different nitrogenous ligands. Once the spectra of [Ni]-BChl at three coordination states were resolved, we could derive the corresponding changes in electronegativity, effective charge, and the covalent radius of Ni(II) by using eqs 7 and 8. Table 2 presents the values derived for each coordination state and ligand.

There is a good correlation between the changes in effective positive charge of Ni(II) upon axial ligation, the number of axial ligands per metal center, and the electron donor properties of each ligand. Specifically, (i) the stronger nucleophile, Im, donates about 10% more negative charge than the weaker one, Py, and (ii) adding a second ligand almost doubles the effect of the first one, for both Im and Py. These observations support our assumption that the effective positive charge at the metal center becomes partly screened because of net electron density migration from the ligand to the [Ni]-BChl central core. The results of the empirical approach and the HDFT/MK-ESP calculations for [Ni]-BChl·Im are in very good agreement. Both methods indicate migration of negative charge from the Im moiety to the [Ni]-BChl upon ligation (0.3 vs 0.21 electron charge units) as well as an increase of the metal's covalent radius (0.07 vs 0.085 Å). Moreover, the HDFT calculations support the assumption that the negative charge is mostly localized at the molecule's central core. The difference between the deficiency of electron density at the Im ligand (0.23 e^-) and the excess density at the [Ni]-BChl core (0.21 e^-) indicates that practically no electron density has been transferred to the BChl π-electron system. Additional experiments and corresponding HDFT calculations on [Ni]-BChl with several other ligands are currently being carried out in our labs.

The experimental approach presented in this paper predicts a similar increase in the net electronic charge around the metal center (0.3 and 0.27 electron charge units for axial ligation of Im and Py to [Ni]-BChl, respectively). The good agreement between high-level HDFT calculations and our empirical derivation of partial charges as described here has encouraged us to apply the empirical approach for studying complex biological systems where ab initio methods are not directly feasible. Furthermore, whereas ab initio calculation is the most rigorous theoretical approach, our empirical method based on electronegativity equalization offers both a quantitative description of charge distribution within a molecule and an understanding of the driving force for this distribution. Since partial atomic charges are not quantum mechanical observables,[50,59] a systematic application of our approach to various ligands will provide an experimental point of reference for different computational techniques whose aim is to resolve charge distribution among atoms in molecules. An extensive computational and experimental study of [Ni]-BChl with a series of axial ligands follows.

Excited-State Dynamics and Axial Ligand Photodissociation. Recently, Musewald et al. have studied the photodynamics of [Ni]-BChl in noncoordinating (toluene) and coordinating (Py) solvents by femtosecond time-resolved absorption and fluorescence spectroscopy.[48,60] Their proposed relaxation mechanisms, which borrow from extensive theoretical and experimental studies of photoexcited D_{4h} [Ni]-porphyrins (with and without axial ligands),[7,30,47,58,61−64] suggest that nonligated [Ni]-BChl undergoes ultrafast internal conversion (IC) within ~100 fs from its initial $^1|S_1, {}^1(d^2)\rangle$ state[65] to a $^1|T_1, {}^3(d,d)\rangle$ state. When [Ni]-BChl is axially coordinated, the initial excited state is a triplet $^3|S_1, {}^3(d,d)\rangle$ that relaxes by ultrafast IC to the $^3|T_1, {}^3(d,d)\rangle$ state within ~200 fs, followed by intersystem crossing (ISC) to the $^1|0, {}^1(d^2)\rangle$ state, which is antibonding for the axial ligands, resulting in their dissociation within ~100 ps.

Although the measurements and accompanied analysis significantly contribute to understanding the photophysics of [Ni]-porphyrins, they could not provide information about the lifetime of monoligated [Ni]-BChl which is essential for interpreting the electron and energy transfer in modified photosynthetic RCs and LHCs.[66,67] We have provided such information first by resolving the [Ni]-BChl spectra at three states of coordination and then analyzing the Q_y absorption line shape of each component. Importantly, the results of our line shape analysis are in agreement with the experimental results. The marked Lorentzian character of the Q_y absorption bands (Figure 2) indicates ultrafast excited-state relaxation. The calculated lifetimes of nonligated and biligated [Ni]-BChls (75 and 150−300 fs, respectively) are in good agreement with the measured relaxation times in toluene and Py (100 and 200 fs, respectively), which validates our estimated lifetimes of monoligated [Ni]-BChl (153 ± 6 and 235 ± 10 for Im and Py, respectively).

Photodissociation of axial ligands was evident in the time-resolved difference absorption spectra of [Ni]-BChl in DE/Py. The good separation of the Q_y and Q_x transitions of [Ni]-BChl and their sensitivity to axial ligation enabled observing the increasing absorption bands at 780 and 534 nm, respectively, which reflects the formation of photodissociated [Ni]-BChl. Geminate rebinding of the axial ligands does not seem to occur within the picosecond time range. As indicated by Musewald et al.,[60] the time constant for ground-state recovery is more than 2 ns.

(59) Chermette, H. *J. Comput. Chem.* **1999**, *20*, 129−154.

(60) Musewald, C.; Gilch, P.; Hartwich, G.; Pollinger-Dammer, F.; Scheer, H.; Michel-Beyerle, M. E. *J. Am. Chem. Soc.* **1999**, *121*, 8876−8881.

(61) Eom, H. S.; Jeoung, S. C.; Kim, D.; Ha, J. H.; Kim, Y. R. *J. Phys. Chem. A* **1997**, *101*, 3661−3669.

(62) Kobayashi, T.; Straub, D.; Rentzepis, P. M. *Photochem. Photobiol.* **1979**, *29*, 925−931.

(63) Uesugi, Y.; Mizutani, Y.; Kitagawa, T. *J. Phys. Chem. A* **1998**, *102*, 5809−5815.

(64) Drain, C. M.; Kirmaier, C.; Medforth, C. J.; Nurco, J.; Smith, K. M.; Holten, D. *J. Phys. Chem.* **1996**, *100*, 11984−11993.

(65) The electronic states of [Ni]-BChl are marked $^n|X, {}^m(Y)\rangle$ where X denotes the macrocycle state (0, S, and T for ground, singlet, and triplet excited states, respectively), Y denotes the metal state (d^2 for a doubly occupied d_{z^2} orbital and d,d for singly occupied d_{z^2} and $d_{x^2-y^2}$ orbitals, respectively), and n and m indicate the overall and metal spin multiplicity, respectively.

(66) Hartwich, G.; Friese, M.; Scheer, H.; Ogrodnik, A.; Michel-Beyerle, M. E. *Chem. Phys.* **1995**, *197*, 423−434.

(67) Bandilla, M.; Ucker, B.; Ram, M.; Simonin, I.; Gelhaye, E.; McDermott, G.; Cogdell, R. J.; Scheer, H. *Biochim. Biophys. Acta* **1998**, *1364*, 390−402.

Conclusion

[Ni]-BChl was found in three states of coordination. Axial ligation involves net charge migration from the ligand to the BChl core, thus changing the metal's effective charge. These changes are reflected in the modified spectra of the BChl π-system and can be measured quantitatively. Such measurements open the way for (i) estimating the electronic chemical potential of various ligands including those of biological significance, (ii) accounting for the tuning of metal coenzymes by their protein surrounding, and (iii) estimating the charge density at catalytic metal centers in homogeneous catalysis.

Acknowledgment. This research was supported by a US−Israel binational science foundation grant (9800323), a sonderforschungsbereich grant (533), and the Willstütter-Avron-Minerva foundation for photosynthesis.

JA993761E